Magnetic aftereffects in CoFeB/Ta/CoFeB spin valves of large area

R. Morgunov, Y. Lu, M. Lavanant, T. Fache, X. Deveaux, S. Migot, O. Koplak, A. Talantsev, S. Mangin

Magnetic aftereffects in CoFeB/Ta/CoFeB spin valves of large area

R. Morgunov,[1,2,*] Y. Lu,[3] M. Lavanant,[3] T. Fache,[3] X. Deveaux,[3] S. Migot,[3] O. Koplak,[1] A. Talantsev,[1,4] and S. Mangin[3]

[1]*Institute of Problems of Chemical Physics, 142432, Chernogolovka, Moscow, Russia*

[2]*Tambov State Technical University, 392000, Tambov, Russia*

[3]*Institut Jean Lamour, UMR 7198 CNRS, Université de Lorraine, 54506 Vandoeuvre, Nancy, France*

[4]*Department of Emerging Materials Science, DGIST, 42988, Daegu, South Korea*

(Received 5 February 2017; revised manuscript received 10 July 2017; published 15 August 2017)

Magnetic aftereffect measurements on a synthetic antiferromagnet with strong perpendicular anisotropy are presented. Two types of magnetic transitions are observed in the CoFeB/Ta/CoFeB bilayer where the two ferromagnetic CoFeB layers are antiferromagnetically coupled: the transition from a parallel to an antiparallel CoFeB layers magnetization alignment and the transition between two possible antiparallel magnetization states. Magnetic relaxation measurements show a complete reversal in the case of the transition between the two antiferromagnetic configurations. The experimental data can be well fitted in the frame of extended exponential relaxation using the Fatuzzo-Labrune model. Consequently, the domain nucleation and domain-wall propagation can be studied as a function of temperature and applied field.

DOI: 10.1103/PhysRevB.96.054421

I. INTRODUCTION

Synthetic antiferromagnets (SAFs) with perpendicular anisotropy (p-SAF) have been designed to be used for applications in magnetic memory and data storage elements engineering. Domain-wall dynamics in systems with perpendicular magnetic anisotropy (PMA) attracts much attention for fundamental studies and potential applications [1,2]. Indeed, domain-wall motion in thin magnetic films provides interesting opportunities for the design of high-performance spintronics devices [1] such as racetrack memories [2], domain-wall logic circuits [3], and domain-wall nano-oscillators [4]. One of the physical constraints for fast dynamics is the presence of the Walker breakdown. The Walker limit corresponds to the magnetic field threshold value leading to the decrease of domain-wall velocity under increasing magnetic field [5]. Quite recently, it has been shown through numerical and analytical modeling that the Walker breakdown limit could be extended or completely eliminated in antiferromagnetically coupled magnetic nanowires such as SAF. SAF nanowires would allow high domain-wall velocity driven by field and/or current as compared to conventional nanowires.

In this context, we focused on the analyses of magnetization dynamics in a model CoFeB/Ta/CoFeB bilayer. It consists of two ultrathin antiferromagnetically exchange-coupled ferromagnetic CoFeB layers with strong perpendicular anisotropy. The multilayer stack was grown directly on a GaAs substrate. Quasistatic magnetization versus field hysteresis loops were measured for different temperatures ranging from 5 to 300 K. It allowed a field-temperature (H-T) magnetization switching diagram to be constructed [6]. Now we would like to focus on the magnetization dynamics during the transition from one magnetic state to the other. Domain-wall dynamics in p-SAF systems is very unusual [1,2] and becomes more complicated for multilayered samples.

Another feature of thin spin valves is very unusual exponential relaxation [7] indicating single-potential barrier relief for domain walls. Observation of reversal magnetization dynamics in single ferromagnetic layers and its comparison with that in the double-ferromagnetic-layer system allows one to judge the contribution of the interlayer interaction to domain-wall dynamics.

Many papers are focused on time-dependent switching of the multilayered heterostructure in the nanosecond scale [1–4]. The damping parameter governs effectiveness of switching of Giant Magnetoresistance devices and their convenience for high-frequency readout in the microwave frequency range. The results mentioned above relate to nanosized spin valves designed for memory cells. Reversal magnetization of these small devices obeys the macrospin approach. Meanwhile, magnetic nanoparticles sensor technology requires larger areas of devices for better resolution and sensitivity to magnetic field. The magnetic aftereffect in these structures has a larger time scale and magnetization reversal cannot be considered in terms of the macrospin model only.

In the present paper, we will pay attention to another problem, which dramatically affects the quality of the large ($\sim$1–10 mm^2) area of CoFeB multilayered structures. Thin ferromagnetic layers as well as CoFeB multilayered structures manifest slow magnetic relaxation due to domain-wall dynamics [8]. In [8], magneto-optic Kerr effect (MOKE) microscopy of those samples studied in this paper was reported. This process is very complicated due to the thermally activated character of the domain-wall unpinning, peculiar interaction between ferromagnetic layers, and inhomogeneous distribution of magnetization through the layer [Fig. 1(a)].

In this paper, we present a detailed study of the time-resolved (for time ranging from seconds) response of magnetization in the CoFeB/Ta/CoFeB bilayer and the CoFeB single-layer samples as a function of temperature and applied magnetic field. Similarities and differences between single-layer magnetization reversal and double-layer simultaneous reversal (direct transition between the antiparallel magnetic states: $AP+$ and $AP-$) in the CoFeB/Ta/CoFeB bilayer will be discussed. The goals of the paper are as follows:

*Corresponding author: morgunov2005@yandex.ru

(1) to reveal the effect of interlayer exchange coupling on domain-wall pinning field threshold and thermoactivation analysis of the $AP+ \rightarrow AP-$ transition in the CoFeB/Ta/CoFeB bilayer and CoFeB single layer, and

(2) to distinguish the contributions of domain nucleation and domain-wall propagation to magnetization dynamics in the different transitions in the CoFeB/Ta/CoFeB bilayer and CoFeB single layer.

II. EXPERIMENT

The multilayered systems that consist of MgO(2.5 nm)/CoFeB(1.1 nm)/Ta(0.75 nm)/CoFeB(0.8 nm)/MgO(2.5 nm)/Ta(5 nm) (*bilayer*) and MgO(2.5 nm)/CoFeB(0.8 nm)/MgO(2.5 nm)/Ta(5 nm) (*single layer*) were deposited on the undoped GaAs (001) substrate by magnetron sputtering. Details of growth conditions can be found elsewhere [9,10]. Stoichiometric composition of CoFeB target was $Co_{40}Fe_{40}B_{20}$. The hybridization of the 3*d* orbitals of transition metals (Co, Fe) with the O_{2p} orbitals of MgO provides perpendicular magnetic anisotropy (PMA) at the CoFeB/MgO interface [11]. To enhance PMA, rapid temperature annealing was performed at 250 °C for 3 min to crystallize the CoFeB layer. During this process, diffusing boron was absorbed by the 0.75-nm Ta interlayer, which facilitated antiferromagnetic coupling between the two separated CoFeB layers [11,12]. The plate-shaped sample $0.3 \times 2 \times 2\ mm^3$ in size was studied. Magnetic hysteresis loops and time dependences of sample magnetization were obtained by a MPMS 5XL Quantum Design magnetometer (SQUID). Magnetic field was directed perpendicular to the sample plane in all experiments.

III. RESULTS AND DISCUSSION

A. Magnetic hysteresis and microstructure of the bilayer

We have performed high-resolved scanning transmission electron microscopy (HRSTEM) analysis [Fig. 1(a)]. The large-scale image [inset of Fig. 1(a)] reveals a continuous and homogeneous layer structure. In the small-scale image, we can identify the detailed structure of the bilayer and the thickness of each layer from the image contrast. The CoFeB/Ta interface is quite diffused, which suggests an intermixing or diffusion of

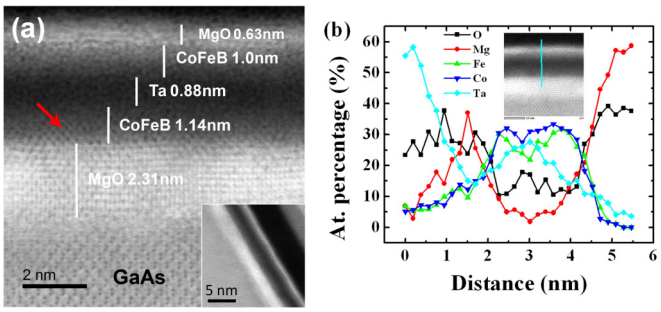

FIG. 1. Structural study of the CoFeB/Ta/CoFeB bilayer. (a) TEM image of the cross section of the sample. Inset: large-scale image of the bilayer. Red arrow corresponds to the location of the EDX profiling. (b) EDX profile. The light blue points in the inset correspond to the scanning points.

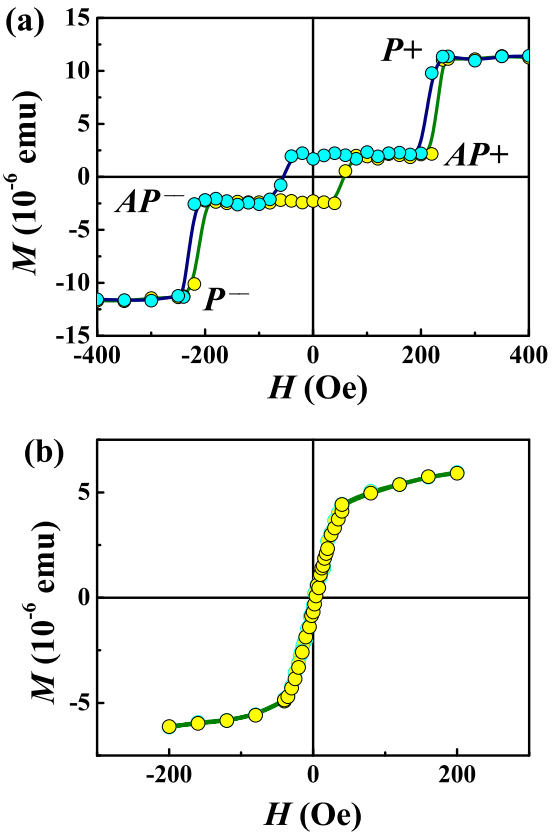

FIG. 2. Magnetization as a function of the magnetic field applied perpendicular to the film plane at 300 K for a bilayer (a) and a single layer (b). Magnetization states of bilayer correspondent to different mutual magnetization orientations of CoFeB layers in the bilayer are marked as $P+$, $AP+$, $AP-$, and $P-$.

Ta in the CoFeB layer after annealing. The thickness of the Ta layer was estimated to be 0.88 ± 0.2 nm, which is in agreement with the nominal thickness of 0.75 nm. In addition, the red arrow points out the beginning of the crystallization of the CoFeB phase starting from the lower CoFeB/MgO interface.

In addition, energy dispersive x-ray (EDX) analysis was performed to check the chemical distribution of the sample, which is shown in Fig. 1(b). The inset of Fig. 1(b) indicates the position of each analyzed point on the section profile. Spatial resolution is better than 0.2 nm. As shown in Fig. 1(b), the broad peak of Ta accompanied by small dips of Co and Fe proves that a strong interdiffusion between Ta and Co (Fe) happens after annealing at 250 °C.

Figure 2(a) shows the magnetic hysteresis loop of the CoFeB/Ta/CoFeB bilayer at $T = 300$ K for magnetic field applied perpendicular to the film plane. Four states, $P+$, $AP+$, $AP-$, and $P-$, correspond to either parallel alignment of the thick (1.1 nm) and thin (0.8 nm) CoFeB layers magnetizations for $P+$ and $P-$ or an antiparallel alignment of the two magnetizations, $AP+$ and $AP-$. The inner loop with $H_{C1} = 40$ Oe coercivity is formed due to the $AP+ \leftrightarrow AP-$ transitions. The outer loops with $H_{C2} \sim 5$ Oe coercivity are formed by $P+ \leftrightarrow AP+$ and $AP- \leftrightarrow P-$ transitions. The centers of these loops are shifted to $\pm H_B = \pm 200$ Oe due

to negative exchange coupling between the two layers as discussed in our previous work [6].

In this paper, we will discuss dynamics of $AP+ \leftrightarrow AP-$ transitions for different magnetic fields and temperatures. The width of the hysteresis loop depends on the relation between the magnetic field sweeping rate and the magnetization dynamic. In the 240–300 K temperature range, $P+ \leftrightarrow AP+$ and $AP- \leftrightarrow P-$ transitions corresponding to the reversal of one of the two ferromagnetic layers were not accompanied by hysteresis (or a very narrow hysteresis loop), while $AP+ \leftrightarrow AP-$ transitions corresponding to simultaneous switching of the two layers show larger hysteresis. The temperature dependences of coercive and bias fields of the subloops are discussed in our previous work [6]. The following dynamic measurements tend to distinguish the characteristic of the two reversals.

The magnetic hysteresis loop of the single CoFeB layer is presented in Fig. 2(b). Despite the fact the magnetization is saturated at $H > 30$ Oe, the magnetocrystalline anisotropy is too weak to induce perpendicular magnetization at zero field. The magnetization is linear with field around zero field and the coercivity at 300 K is zero.

B. Competition between domain nucleation and domain-wall propagation contributions in magnetization transitions

Time dependences of reversal magnetization accompanying $AP+ \leftrightarrow AP-$ transitions in the bilayer were recorded in accordance with the procedure schematically depicted in the upper panel of Fig. 3(a).

At the first stage, the sample was magnetized in field $H = 1$ kOe exceeding saturation magnetic field H_S. The magnetic field was perpendicular to the film (i.e., along the easy magnetization axis). The duration of the magnetization stage was 300 s. Thus the initial magnetic state of the bilayer was unified in all experiments. At the second stage, the magnetic field H_S was turned to the H^* value below H_S. The duration of the magnetic field switching ("dead time") was 60 s. Immediately after stabilization of the H^* value, the record of the time dependence of magnetic moment M was started ($t = 0$). The response of the sample magnetization to stepwise changes in magnetic field is shown in the bottom panel of Fig. 3(a). The magnetic field switching to the H^* values corresponding to out-of-loop parts of the $M(H)$ dependence does not initiate magnetic relaxation. The record time for the $M(t)$ dependence was 3600 s. More than ten cycles of the above-described sequence were carried out at different magnetic fields lying in the $H^* = -1$ to $+1$ kOe range. The above-described sequences were repeated in the 240–350 K temperature range. The values of relaxation depths and times obtained by this method can also be found from the first order reversal curve (FORC) diagrams [13–15]. However, in the FORC technique time dependence of magnetization is recorded while sweeping the magnetic field. In our case recording of $M(t)$ dependence was performed in a stationary magnetic field. Additional information on the use of this technique can be found in [16].

In Fig. 3(b), time dependences of the magnetization of the bilayer are shown in magnetic fields H^* close to the H_{C1} and $\pm H_B \pm H_{C2}$ values: from +210 to + 200 Oe for the $P+ \rightarrow$

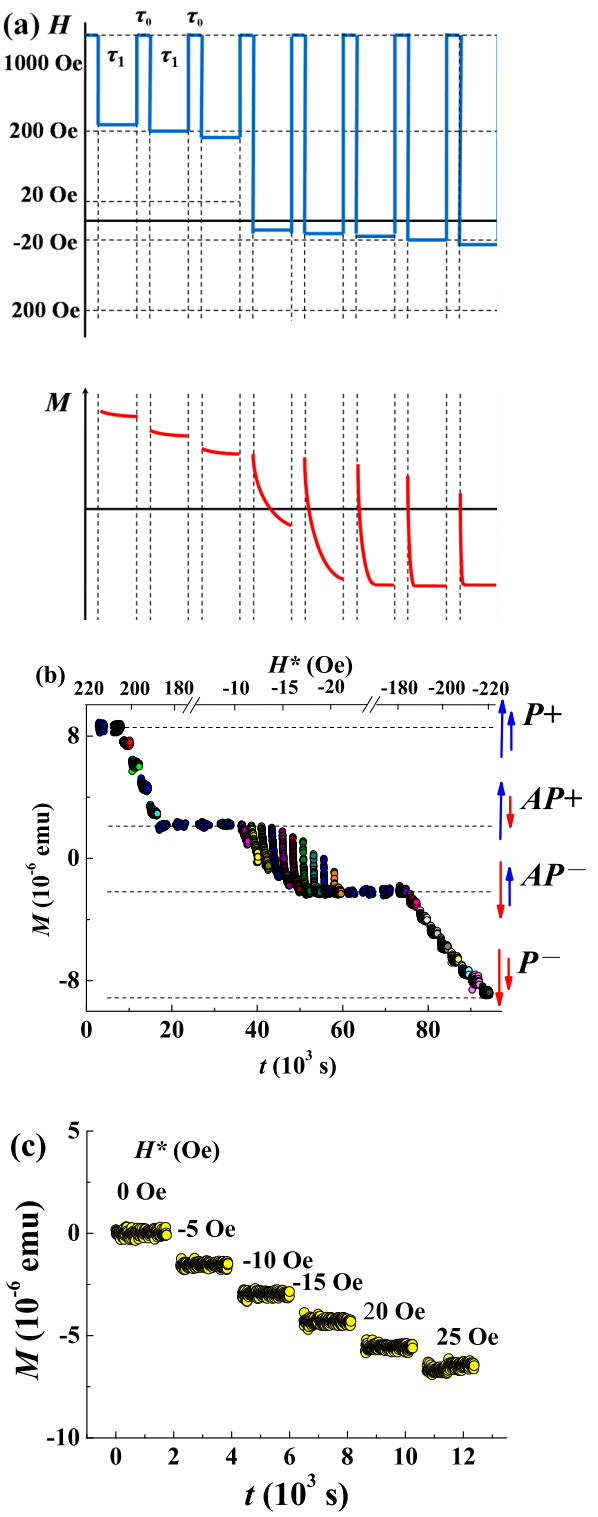

FIG. 3. (a) The scheme of magnetic relaxation recording. The upper panel is a sequence of magnetic field switching, and the lower panel shows correspondent magnetic moment responses. (b) Time dependences of magnetic moment M for the bilayer recorded at $T = 300$ K in magnetic fields H^* lying in the range from –210 to +210 Oe. Blue and red arrows on the right panel indicate directions of magnetization of the ferromagnetic layers in different states, $P+, AP+, AP-$, and $P-$. (c) Time dependences of magnetic moment M for the single layer in 0 to –25 Oe reversal magnetic field.

$AP+$ transition, from –13 to –22 Oe for the $AP+ \rightarrow AP-$ transition, and from –200 to –210 Oe for the $AP- \rightarrow P-$ transition. No time dependences were found in magnetic fields H^* close to $P+ \rightarrow AP+$ and $AP- \rightarrow P-$ transitions. Most probably magnetic relaxation was finished within the period of magnetic field stabilization (∼1 min). In contrast to the bilayer, the single layer demonstrates no relaxation behavior in the entire $H^* = -1$ to $+1$ kOe range. Several time dependences of magnetization for the single layer in reversal magnetic field H^* are given in Fig. 3(c).

These time dependences for the single layer start from the different value of magnetization dependent on the reversal magnetic field. Since magnetization does not change with time, one can assume that magnetic relaxation was finished before the measurements were started. Later we will discuss magnetic relaxation of the bilayer sample only.

Complete magnetization reversal from the $AP+$ to the $AP-$ state is demonstrated for a bilayer in the –13 to –22 Oe magnetic field range: all time dependences were started from the same M_{AP+} value and finished close to the M_{AP-} value.

These dependences are different from each other in velocity of the $AP+ \rightarrow AP-$ transitions, which increases as absolute H^* value increases.

Five different models to describe the magnetic relaxation are proposed in the literature.

(1) Exponential law (Debye relaxation): $M(t) = M_0\exp(-t/\tau)$ is valid for single particles or films with single-barrier, narrow distribution of energy barriers for the domain nucleation and propagation (see [17] for both).

(2) Logarithmic law: $M(t) = M_0 - S(H,T)\ln(t/t_0)$ for magnetic films with in-plane anisotropy [17] and $M(t) = M_0 - S(H,T)\ln(1 + t/t_0)$ for the films with perpendicular anisotropy [18,19]. The time dependence of magnetization can be described by the logarithmic law, when the energy distribution of the barrier heights is large. The wider the energy distribution the better the quality of the approximation by the logarithmic law [20].

(3) Power law relaxation $M(t) = M_0 t^{-\zeta}$, $\zeta < 1$. This type of relaxation has been observed in spin glasses such as the γ-FeNiCr alloys [21] and in single-domain ferromagnetic nanoparticles [22]. This behavior can be understood in the context of the flipping of spin clusters [23].

(4) Stretched exponential relaxation $M(t) = M_0\exp[-(t/\tau)^{\beta}]$, $\beta < 1$ (Kohlrausch-Williams-Watts stretched exponential decay). This type of relaxation was observed in the films with log-normal distribution of the energy barrier heights [24], as well as in a variety of clusters, amorphous materials, strongly disordered films, and spin glasses [25–32]. This relaxation is slower than the conventional exponential decay ($\beta = 1$), since the system goes through metastable states during the process towards the ultimate thermal equilibrium [20,33].

(5) Compressed exponent relaxation $M(t) = M_0\exp[-(t/\tau)^{\beta}]$, $1 < \beta < 3$ (Kolmogorov-Avrami-Fatuzzo relaxation). This model can be applied for the relaxation in spin glasses and in thin films and multilayers as well. As for the films, the following description of the model can be found [34]. Demagnetization of the film results in first some reversed spins or grains appearing in the film. The short-ranged exchange coupling makes the adjacent spins or grains more likely to reverse than the others. The latter results in the formation of magnetic domains and their growth over time from the reversed spins or grains, which are considered as nuclei [20]. That is why the compressed exponent model can be applied to the magnetization relaxation in thin films, when the magnetization reversal is governed by domain nucleation and is accelerated by domain propagation. The value of the exponent β depends on the dimensionality of the domain motion as well as on the homogeneity of the film. The $\beta = 1$ corresponds to negligible domain propagation contribution; $\beta = 3$ corresponds to three-dimensional domain propagation in films of high homogeneity in the case when the domain propagation contribution to the magnetization reversal is dominant.

Approximations of the time dependences by first three models, mentioned above, are presented in Fig. S1 of the Supplemental Material [35]. Magnetic field and temperature dependences of the relaxation time from the exponential relaxation model may be treated in terms of classical thermoactivation analysis. The straightening of magnetic field dependences of the relaxation time in $T\ln(\Gamma_0/\Gamma)$ versus H coordinates ($\Gamma = 1/\tau$, τ is the relaxation time, and Γ_0 is the frequency factor) is presented in Fig. S2 of the Supplemental Material [35]. However, this model gives an unreasonably high value of the frequency factor $\Gamma_0 \sim 10^{25}$ Hz. That means the single-barrier relaxation model is not applicable in our case because of wide distribution of the domain-wall depinning barrier heights in the bilayer sample.

The last model can be rewritten in terms of the competition between domain nucleation and domain-wall (DW) motion [34,36–38]:

$$\begin{aligned}[M(t) + M_S]/2M_S &= \exp\{-k^2[2 - 2(Rt + k^{-1}) + (Rt + k^{-1})^2 \\ &\quad - 2e^{-Rt}(1-k^{-1}) - k^{-2}(1 - Rt)]\}, \end{aligned} \tag{1}$$

where R is the probability of nucleation per time unit, and $k = v/Rr_0$ is the relation between DW velocity v and the product of nucleation frequency R, and the initial radius of nuclei r_0 is a dimensionless parameter, which characterizes a competition between DW propagation and nucleation of domains. This type of the compressed exponent model is referred to as the Fatuzzo-Labrune model.

Thus a set of magnetic relaxation curves at different magnetic fields H and temperatures T can be recalculated in the dependences of nucleation probability and domain-wall velocity on magnetic field and temperature. According to [39], the exponential growth of v with the magnetic field corresponds to thermoactivated DW motion, while linear dependence $v(H)$ corresponds to viscous DW motion. The saturation of $v(H)$ dependence corresponds to the Walker limit, wherein DW velocity is magnetic field independent or decreases as field increases.

First we will discuss the dynamics of the $AP+ \rightarrow AP-$ flop transition accompanied by remagnetization of both ferromagnetic layers. Examples of approximation of time dependences $M(t)$ at 240 and 300 K by Eq. (1) are presented in Fig. 4. All sets of the magnetic relaxation curves from 240 to 320 K with a 10 K temperature step, recorded under 6 to 55

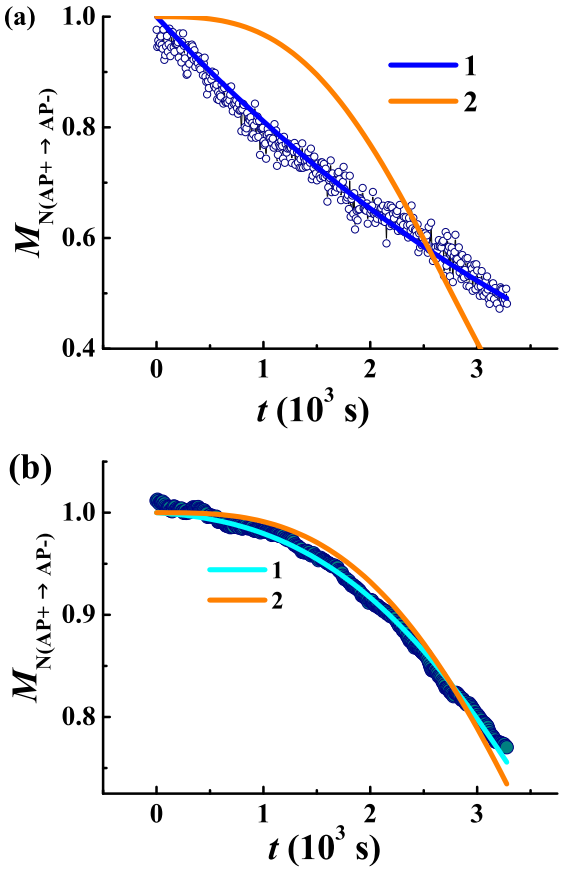

FIG. 4. Time dependences of magnetization at 300 K (a) and 240 K (b) for the same $\tau_{1/2}$ value, and their approximations in terms of the Fatuzzo-Labrune full (curve 1) and simplified ($k \gg 1$, curve 2) models, $M_{N(AP+\rightarrow AP-)} = [M(t)–M_{AP-})/(M_{AP+}–M_{AP-})$.

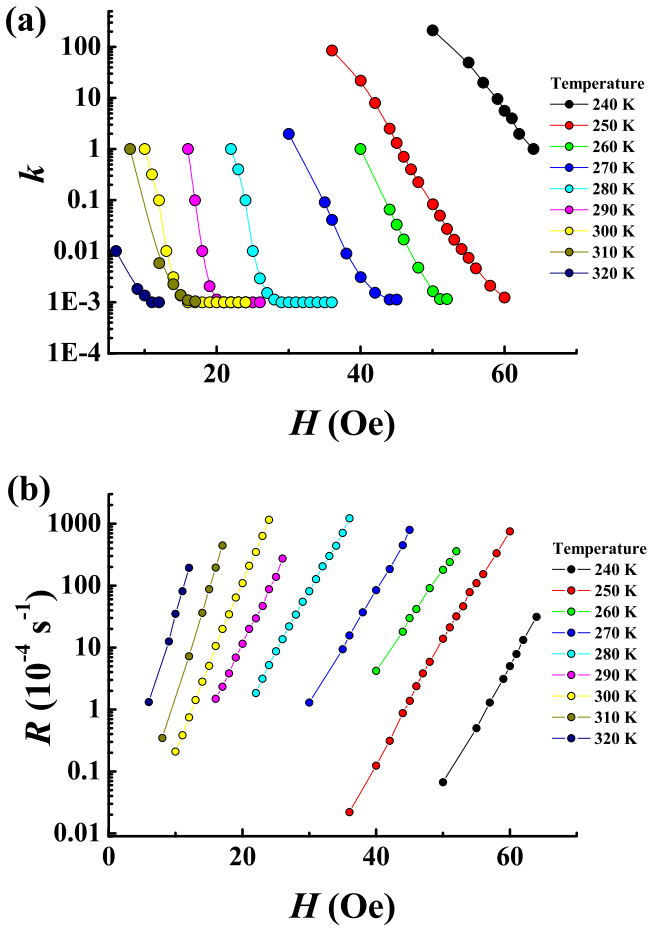

FIG. 5. Magnetic field dependences of propagation constant k (a) and nucleation probability R (b) in the 240–320 K temperature range.

Oe applied magnetic field with a 1-Oe step, are presented in Fig. S3 of the Supplemental Material [35].

One can see that a temperature decrease changes time dependence from an exponential one $M(t) = \exp(–\alpha t)$ (at 280–300 K) [Fig. 4(a), curve 1] to a power-exponential dependence $M(t) = \exp(–\beta t^3)$ (at 240–270 K) [Fig. 4(b), curve 1].

If DW propagation is a dominant process, Eq. (1) can be rewritten as

$$[M(t) + M_S]/2M_S = \exp[-k^2(Rt)^3/3] \qquad (2)$$

(the simplified Fatuzzo-Labrune model).

Approximations of $M(t)$ by Eq. (2) are presented in Figs. 4(a) and 4(b), curve 2. At low temperatures (240–270 K) this approximation coincides well with the experimental data, and at high temperatures (280–300 K), no satisfactory approximation can be reached. Thus the contribution of DW propagation to reversal magnetization increases at low temperatures.

In the frame of the Fatuzzo-Labrune model, we will determine the proportion of reversal nucleation and DW propagation to reversal magnetization of the bilayer. The k parameter corresponds to this proportion. If nucleation is dominant, the k value is close to zero, while its value increases up to ~1–100 [37] corresponding to DW propagation being the main reason for magnetic relaxation. In our experiments at low temperatures 240–270 K, $k \sim$ 1–100; i.e., DW propagation is dominant [Fig. 5(a)]. On the contrary, the k value is very small ($k \ll 1$) at 280–300 K, which indicates domination of the nucleation mechanism (bilayer sample).

Dependences of parameter R on magnetic field are shown in Fig. 5(b) for different temperatures.

In terms of the Fatuzzo-Labrune model, the nucleation probability depends on temperature T and applied magnetic field H as follows:

$$R(T,H) = R_0 \exp[-(W_N - 2HM_S V_N)/k_B T], \qquad (3)$$

where W_N is the energy barrier and V_N is the activation volume for the nucleation process.

Equation (3) can be rewritten as

$$k_B T \ln[R(T,H)] = A + BH, \qquad (3')$$

where $A = -W_N + k_B T \ln(R_0), B = 2M_S V_N$.

Magnetic field dependences of R were approximated by (3′) and the values of A and B were extracted at each temperature. Temperature dependences of parameter A and activation volume V_N are presented in Figs. 6(a) and 6(b), respectively. The linear approximation of $A(T)$ dependence at 280–320 K [line 1, Fig. 6(a)] allows us to determine

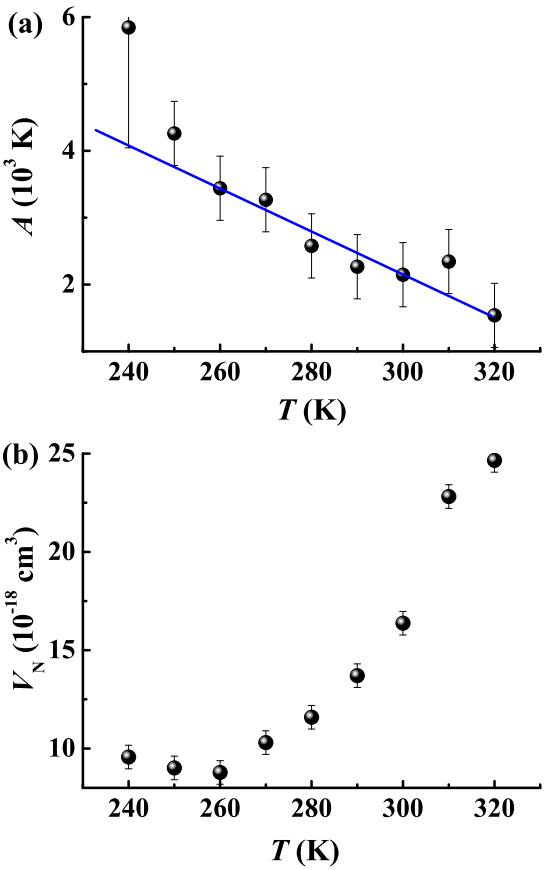

FIG. 6. Temperature dependences of parameter A [$A = W - T\ln(R_0)$; W is the nucleation energy barrier, R_0 is the nucleation frequency factor] (a), and activation volume V_N (b). Solid line is linear approximation.

energy barrier $W \sim 8.2 \times 10^3$ K and nucleation frequency factor $R_0 \sim 10^8 s^{-1}$.

At lower temperatures, the deviation of $A(T)$ dependence from a straight line is caused by the increase in propagation contribution in agreement with our previous conclusions. The linear size of the activation area l_N can be estimated from V_N value: $l_N \sim (V_N/\pi h)^{1/2} \sim 80$ nm is comparable with typical values of domain widths in thin CoFeB films [40].

Thus the Fatuzzo-Labrune model gives reasonable values for nucleation energy barrier, frequency factor, and activation volume. This model also gives qualitative information on the contribution of the domain-wall propagation. However, the domain propagation coefficient k strongly depends on magnetic field [Fig. 5(a)], which is in contradiction with previous results obtained for magnetic layers with perpendicular anisotropy [6,39,41]. This contradiction can be overcome in the frame of the extended exponential relaxation model, where magnetic relaxation is described by the following equation [20]:

$$M(t) = M_0 \exp[-(t/\tau)^{\beta}]. \quad (4)$$

The case $\beta = 1$ corresponds to Debye relaxation, $\beta < 1$ to the stretched exponent, and $\beta > 1$ to the compressed exponent model.

Magnetic relaxation time τ dependences on temperature and magnetic field are presented in Fig. 7. One can see a quite

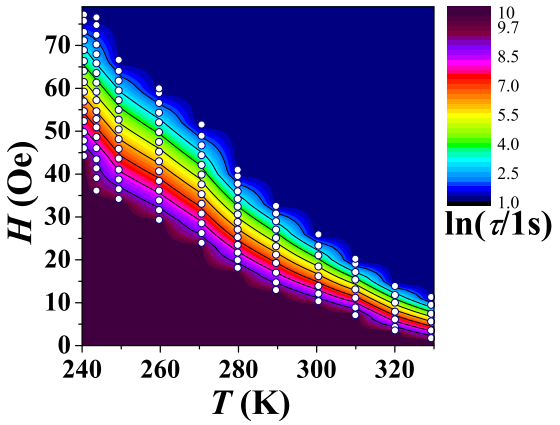

FIG. 7. H-T diagram of the relaxation time τ. The color scale corresponds to the value of the relaxation time $\ln(\tau/1\,\mathrm{s})$, determined from the extended exponential relaxation model. The open symbols on the diagram are experimental points.

narrow interval of magnetic fields, where relaxation times are in the 1–1000 s range. This interval moves to higher magnetic fields at lower temperatures.

The $\beta(H, T)$ dependences are presented in Fig. 8. One can see that $\beta(H,T)$ increases with a decrease of temperature. Furthermore, $\beta > 1$ for the entire magnetic field range at low temperatures (240–250 K), while at higher temperatures β becomes smaller than 1, when the magnetic field increases. An increase of temperature results in the widening of the magnetic field range, correspondent to $\beta < 1$. Here we will provide one possible explanation of the effect. Basically, one can distinguish three stages of the magnetization reversal in the bilayer. The first stage is the formation of a few nuclei of reversed magnetization in the top and bottom layers. The second stage is the growth of these nuclei due to the domain propagation, as well as the formation of new nuclei. The magnetic reversal velocity dM/dt, being proportional to the l^2/S ratio (l is the total length of the domain walls; S is the total area of the reversed domains), increases until reversed domains contact and coalesce with each other. The last stage begins when reversed domains start to coalesce.

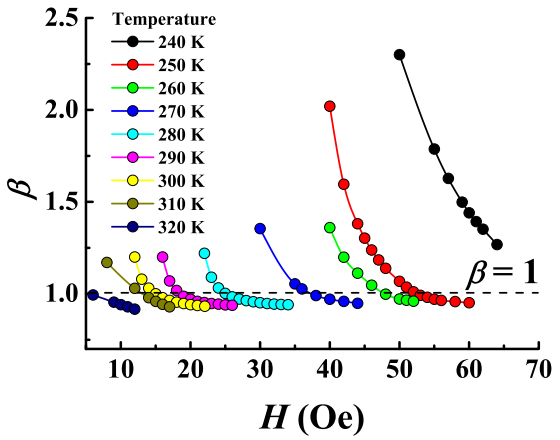

FIG. 8. Magnetic field dependences of exponent β at 240–320 K temperature range.

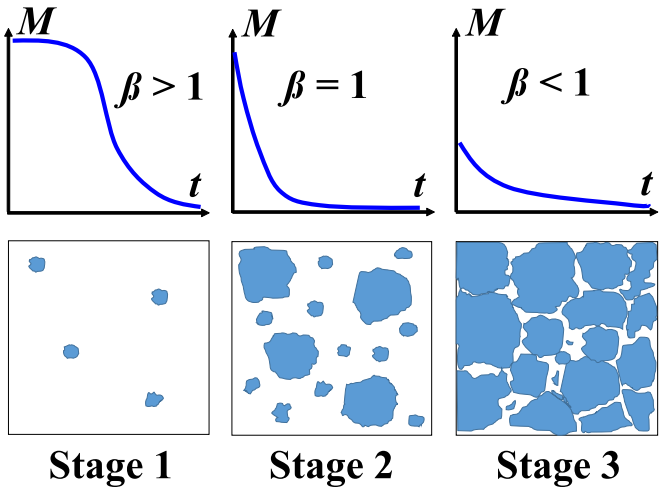

FIG. 9. Sketch of the $M(t)$ curves (top panel) and the correspondent reversed magnetization areas (dark spots) in the bilayer (bottom panel) for three stages of magnetization reversal, described in the text.

This stage is accompanied with a decrease of the l^2/S ratio and the correspondent decrease of dM/dt. Furthermore, magnetic relaxation at the last stage becomes slower than the expected exponential relaxation due to the formation of nonreversed magnetic "bubbles." The bubble contains two coalesced domains. It appears when the domain passes around a pinning site or void (Fig. 9). This fact was confirmed by direct MOKE measurements in [8]. The bubbles can be stabilized by the demagnetizing field generated by the surface magnetic charge against the applied field [20,42]. The magnetization dynamics associated with these bubbles is similar to that described by the droplet and domain models [43,44] in spin glasses. Therefore, domain growth and bubble reversal both contribute to the relaxation.

The ratio between the durations of these stages is dependent on applied magnetic field. For the lower fields and lower temperatures, the first and the second stages are longer, and almost complete magnetization reversal happens before the third stage begins. That is why $\beta > 1$ for small applied fields (long relaxation times) in the entire temperature range. An increase of applied field results in the shortening of the first and second stages in comparison with the third stage due to an increase of the nucleation frequency. This competition results in a decrease of β. The "dead" time of reversal magnetic field switching (~60 s) becomes comparable with magnetic relaxation time τ when it decreases from several hours down to a few minutes. The last circumstance results in the completion of the first and second stages of the relaxation within the dead time, i.e., before the recording of the $M(t)$ dependence is started. In that case recorded $M(t)$ dependence will contain the third stage of the magnetization reversal only (with $\beta < 1$ stretched exponential decay). Domains stop growing and bubble reversal becomes dominant in the late phase of the process.

Thus variations of magnetic field and temperature allow adjustment of the time "window" of the experiment to resolve first ($\beta > 1$), second ($\beta = 1$), and third ($\beta < 1$) stages of magnetic relaxation separately from each other.

The further temperature decrease down to 100 K results in changes in the transition sequence, and $AP+ \rightarrow AP-$ transition becomes impossible. However, only two transitions (instead of three at 300 K) occur on the major hysteresis loop: $P+ \rightarrow AP-$ and $AP+ \rightarrow P-$ [6].

One can also observe an $AP+ \rightarrow P-$ transition on the minor hysteresis loop, if the bilayer sample was previously cooled down to 100 K under the $AP+$ state [6]. Here we will discuss $P+ \rightarrow AP-$ and $AP+ \rightarrow P-$, corresponding to the switching of a single top or bottom layer magnetization. The comparison of the bottom layer $M(t)$ curves at $P+ \rightarrow AP-$ and $AP+ \rightarrow P-$ transitions for a single layer in the bilayer and $M(t)$ curves for the single layer are presented in Figs. 10(a)–10(c), respectively. These three sets of curves look similar manifesting low k values ($k \sim 0.001$ or less) for the entire magnetic field range. That means $P+ \rightarrow AP-$ is governed by nucleation only, while the contribution of the DW propagation is negligible.

Magnetic field dependence of R value is presented in Fig. 11. In contrast to high-temperature results, the semilogarithmical $R(H)$ dependence is not linear at low temperatures. The range of switching magnetic field for the thick bottom layer in the bilayer depends on the magnetization direction of the upper layer M_U with respect to the magnetization of the bottom layer M_D. In the $P+$ state, magnetizations of both ferromagnetic layers have the same direction. Demagnetization from $P+$ state caused by the decrease of magnetic field is accompanied by the reversal of the bottom layer in positive magnetic fields from +100 Oe to +20 Oe, due to the interlayer antiferromagnetic exchange coupling. The switching rate rises when the external magnetic field decreases.

Remagnetization of the bottom layer from the $AP-$ state implying opposite directions of the M_U and M_D magnetizations takes place at negative magnetic fields between –300 Oe and –200 Oe in the bilayer (Fig. 11, curve 2). Switching fields for the single layer are in the –100 Oe to –150 Oe range, because the antiferromagnetic interlayer exchange impedes the transition (Fig. 11, curve 3).

The $R(H)$ dependence for the single layer lies between relaxation curves from $P+$ and $AP+$ states in the bilayer. Thus, in the case of unidirected M_U and M_D vectors, the antiferromagnetic exchange interaction facilitates the magnetization reversal of the bottom layer, shifting switching fields to positive values, while in the case of oppositely directed M_U and M_D vectors, antiferromagnetic exchange impedes magnetization reversal of the bottom layer, shifting switching external fields to positive values.

In accordance with our previous work [6], the interlayer exchange interaction E_{EX} corresponds to an additional effective magnetic field $\pm H_{eff} = E_{EX}/M_D$. The $R(H)$ dependences were replotted in other coordinates $R(|H - H_{EX}|)$ in Fig. 12. One can see that correction of the external magnetic field by the addition of an effective magnetic field leads to the approaching of $R(H)$ dependences of all three curves to each other. Thus the effective magnetic field unifies $R(H)$ dependences for reversal magnetization of the $P+$ state (curve 1) and $AP+$ state (curve 2) and single layer (curve 3). The small differences between the curves in Fig. 12 can be explained by the difference of the magnetic anisotropy in the above-discussed layers.

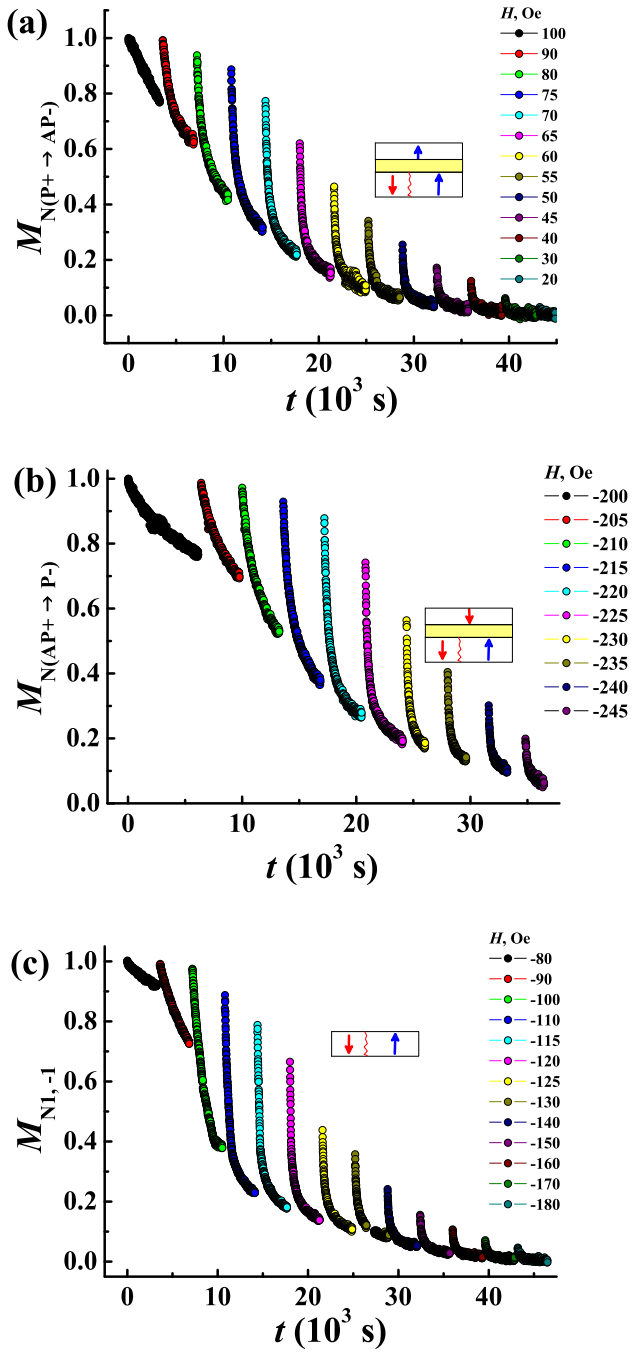

FIG. 10. Time dependences of the bottom layer magnetization at 100 K from $P+$ (a) and $AP+$ (b) states for the bilayer and from the spin-up state for the single layer (c). Magnetic configurations of the layers are presented schematically as insets. $M_{N(P+\rightarrow AP-)} = [M(t)-M_{AP-}]/(M_{P+}-M_{AP-})$ (a), $M_{N(AP+\rightarrow P-)} = (M(t)-M_{P-})/(M_{AP+}-M_{P-})$ (b), $M_{N1,-1} = [M(t)+M_S]/2M_S$ (c).

The experimental technique described above can be considered as the development of the famous modern method of studying magnetic relaxation (FORC) [13–15]. Multiple measurements of magnetic relaxation in different conditions (field and temperature) can provide a 2D map of relaxation parameters in the case of the unified approach for their extraction. Instead of mapping the FORC parameters every relaxation curve was treated individually to judge the physical origin of magnetic relaxation, while FORC allows one to distinguish the presence of only a few mechanisms.

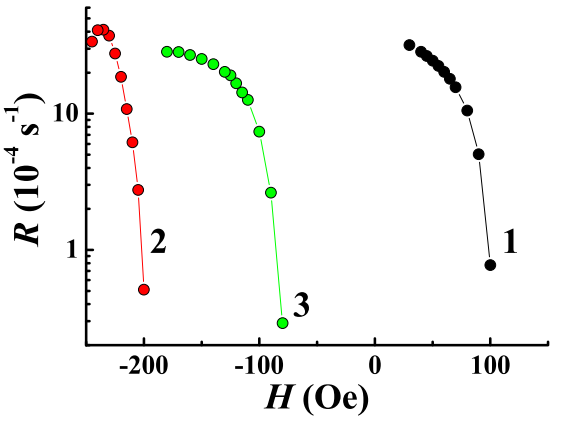

FIG. 11. Magnetic field dependences of nucleation probability at 100 K for the bottom layer of the bilayer [$P+ \rightarrow AP-$ (curve 1) and $AP+ \rightarrow P-$ (curve 2) transitions] and for the single layer (curve 3).

IV. CONCLUSIONS

In a CoFeB/Ta/CoFeB bilayer two types of magnetization reversals are demonstrated: single-layer reversal at the transitions between parallel and antiparallel states and bilayer reversal between the two antiparallel states.

Magnetic aftereffects for the two types of reversal are found to be of different origin. P to AP transitions dynamics in the bilayer is governed by domain nucleation only in the entire 100–320 K temperature range. Reversal between the two antiferromagnetic configurations is governed both by domain nucleation and domain-wall propagation. The decrease of temperature enforces the domain-wall propagation contribution.

Three stages of the flop magnetization reversal between two antiparallel states of the bilayer are revealed. These stages can be identified by the β parameter value obtained in frames of extended exponential relaxation model. The first stage

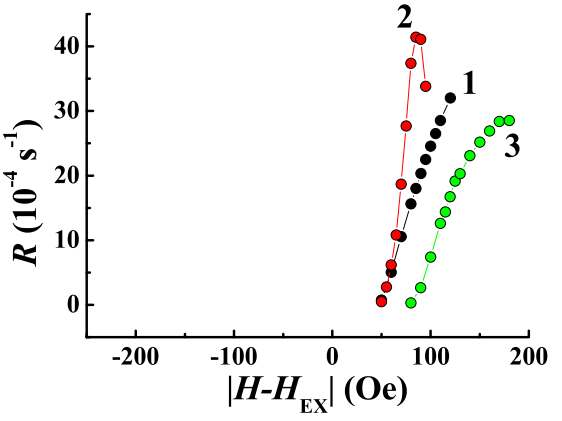

FIG. 12. Magnetic field dependences of nucleation frequency in $(R, |H-H_{EX}|)$ scale.

($\beta > 1$) is characterized by the formation of a few areas of reversed magnetization and their growth, proportional to the square of the domain-wall velocity. The second stage ($\beta \sim 1$) is characterized by a lot of reversed magnetization areas of different sizes and comparable contribution of domain nucleation and domain-wall propagation to magnetization reversal dynamics. The third stage ($\beta < 1$) corresponds to coalescence of reversed magnetization areas. Formation of nonreversed magnetic "bubbles," happens when the domain passes around a pinning site or a void results in retardation of magnetization reversal. Variations of temperature and magnetic field allow the adjustment of the time window of the experiment to record all three stages of magnetization reversal separately from each other. An increase of applied magnetic field as well as an increase of temperature results in a shortening of the first and second stages in the 240–320 K temperature range.

ACKNOWLEDGMENTS

This work was supported by the Ministry of Education and Science of the Russian Federation (Grant No. 3.1992.2017/PCh), the joint French National Research Agency (ANR), the National Natural Science Foundation of China (NSFC) SISTER project (Grants No. ANR-11-IS10-0001 and No. NNSFC 61161130527), and the ENSEMBLE project (Grants No. ANR-14-0028-01 and No. NNSFC 61411136001), as well as by Région Lorraine. Support was also received through ANR-NSF Project No. ANR-13-IS04-0008-01, COMAG, the ANR-Labcom Project LSTNM, and the Université de la Grande Region. Experiments were performed using equipment from the TUBE–Davm funded by FEDER (EU), ANR, Région Grand Est, and Grand Nancy. This work was supported partly by the French PIA project "Lorraine Université d'Excellence," Reference No. ANR-15-IDEX-04-LUE

[1] M. Raju, N. Behera, D. K. Pandya, and S. Chaudhary, J. Appl. Phys. **115**, 17D127 (2014).
[2] X. Liu, W. Zhang, M. J. Carter, and G. Xiao, J. Appl. Phys. **110**, 033910 (2011).
[3] S. Iihama, S. Mizukami, H. Naganuma, M. Oogane, Y. Ando, and T. Miyazaki, Phys. Rev. B **89**, 174416 (2014).
[4] W. He, T. Zhu, X. Q. Zhang, H. T. Yang, and Z. H. Cheng, Sci. Rep. **3**, 2883 (2013).
[5] S. Glathe, R. Mattheis, and D. V. Berkov, Appl. Phys. Lett. **93**, 072508 (2008).
[6] O. Koplak, A. Talantsev, Y. Lu, A. Hamadeh, P. Pirro, T. Hauet, R. Morgunov, and S. Mangin, J. Magn. Magn. Mater. **433**, 91 (2017).
[7] S. Mangin, A. Sulpice, G. Marchal, C. Bellouard, W. Wernsdorfer, and B. Barbara, Phys. Rev. B **60**, 1204 (1999).
[8] M. Lavanant, S. Petit-Watelot, A. D. Kent, and S. Mangin, J. Magn. Magn. Mater. **428**, 293 (2017).
[9] B. S. Tao, P. Barate, J. Frougier, P. Renucci, B. Xu, A. Djeffal, H. Jaffrès, J.-M. George, X. Marie, S. Petit-Watelot, S. Mangin, X. F. Han, Z. G. Wang, and Y. Lu, Appl. Phys. Lett. **108**, 152404 (2016).
[10] S. H. Liang, T. T. Zhang, P. Barate, J. Frougier, M. Vidal, P. Renucci, B. Xu, H. Jaffrès, J. M. George, X. Devaux, M. Hehn, X. Marie, S. Mangin, H. X. Yang, A. Hallal, M. Chshiev, T. Amand, H. F. Liu, D. P. Liu, X. F. Han *et al.*, Phys. Rev. B **90**, 085310 (2014).
[11] H. X. Yang, M. Chshiev, B. Dieny, J. H. Lee, A. Manchon, and K. H. Shin, Phys. Rev. B **84**, 054401 (2011).
[12] C.-W. Cheng, C.H. Shiue, T.-I. Cheng, and G. Chern, J. Appl. Phys. **112**, 033917 (2012).
[13] C. R. Pike, C. A. Ross, R. T. Scalettar, and G. Zimanyi, Phys. Rev. B **71**, 134407 (2005).
[14] D. Cimpoesu, I. Dumitru, and A. Stancu, J. Appl. Phys. **120**, 173902 (2016).
[15] M. Pan, P. Zhang, H. Ge, N. Yu, and Q. Wu, J. Magn. Magn. Mater. **361**, 219 (2014).
[16] A. Talantsev, O. Koplak, and R. Morgunov, Superlattices Microstruct. **95**, 14 (2016).
[17] S. Chikazumi, *Physics of Ferromagnetism*, 2nd ed. (Clarendon, Oxford, 1997), p. 541.
[18] W. Jiang, N. Smith, M. Williams, W. Weresin, K. Kuroki, Y. Ikeda, K. Takano, G. Khera, and R. Wood, IEEE Trans. Magn. **39**, 1891 (2003).
[19] R. Prozorov, Y. Yeshurun, T. Prozorov, and A. Gedanken, Phys. Rev. B **59**, 6956 (1999).
[20] H. Xi, K.-Z. Gao, J. Ouyang, Y. Shi, and Y. Yang, J. Phys.: Condens. Matter **20**, 295220 (2008).
[21] G. Sinha, R. Chatterjee, M. Uehara, and A. K. Majumdar, J. Magn. Magn. Mater. **164**, 345 (1996).
[22] M. Ulrich, J. Garcia-Otero, J. Rivas, and A. Bunde, Phys. Rev. B **67**, 024416 (2003).
[23] K. Binder and A. P. Young, Rev. Mod. Phys. **58**, 801 (1986).
[24] R. W. Chantrell, A. Lyberatos, M. El-Hilo, and K. O'Grady, J. Appl. Phys. **76**, 6407 (1994).
[25] W. Gotze and L. Sjogren, Rep. Prog. Phys. **55**, 241 (1992), and references therein.
[26] J. C. Phillips, Rep. Prog. Phys. **59**, 1133 (1996), and references therein.
[27] C. A. Angell, K. L. Ngai, G. B. McKenna, P. F. McMillan, and S. W. Martin, J. Appl. Phys. **88**, 3113 (2000).
[28] D. Gatteschi and R. Sessoli, Angew. Chem., Int. Ed. **42**, 268 (2003).
[29] L. Cipelletti and L. Ramos, J. Phys.: Condens. Matter **17**, R253 (2005).
[30] R. V. Chamberlin, G. Mozurkewich and R. Orbach, Phys. Rev. Lett. **52**, 867 (1984).
[31] C. A. Cardoso, F. M. Araujo-Moreira, V. P. S. Awana, E. Takayama-Muromachi, O. F. de Lima, H. Yamauchi, and M. Karppinen, Phys. Rev. B **67**, 020407(R) (2003).
[32] M. D. Mukadam, S. M. Yusuf, P. Sharma, S. K. Kulshreshtha, and G. K. Dey, Phys. Rev. B **72**, 174408 (2005).
[33] D. K. Lottis, R. M. White, and E. D. Dahlberg, Phys. Rev. Lett. **67**, 362 (1991).
[34] E. Fatuzzo, Phys. Rev. **127**, 1999 (1962).
[35] See Supplemental Material at http://link.aps.org/supplemental/10.1103/PhysRevB.96.054421 for (Fig. S1) a comparison of

exponential, logarithmic, and power-law approximations of magnetic relaxation curves; (Fig. S2) straightening of magnetic field dependences of the relaxation time at different frequency factors; (Fig. S3) a series of magnetic relaxation curves in the 240–330 K temperature range.

[36] A. A. Adjanoh, R. Belhi, J. Vogel, M. Ayadi, and K. Abdelmoula, J. Magn. Magn. Mater. **323**, 504 (2011).

[37] M. Labrune, S. Andrieu, F. Rio, and P. Bernstein, J. Magn. Magn. Mater. **80**, 211 (1989).

[38] J. Ferre, in *Spin Dynamics in Confined Magnetic Structures*, edited by B. Hillebrands and K. Ounadjela (Springer, Heidelberg, 2001), p. 127.

[39] J. Pommier, P. Meyer, G. Penissard, J. Ferre, P. Bruno, and D. Renard, Phys. Rev. Lett. **65**, 2054 (1990).

[40] M. Alguero, J. M. Gregg, and L. Mitoseriu, *Nanoscale Ferroelectrics and Multiferroics: Key Processing and Characterization Issues, and Nanoscale Effects* (John Wiley & Sons, Hoboken, NJ, 2016), p. 21-5.

[41] S.-B. Choe and S.-C. Shin, Phys. Rev. B **57**, 1085 (1998).

[42] E. A. Jagla, Phys. Rev. B **72**, 094406 (2005).

[43] D. A. Huse and D. S. Fisher, Phys. Rev. B **35**, 6841 (1987).

[44] G. Koper and H. Hilhorst, J. Phys. (Paris) **49**, 429 (1988).